JGR Atmospheres

RESEARCH ARTICLE
10.1029/2021JD035666

Climatology of Mesosphere and Lower Thermosphere Residual Circulations and Mesopause Height Derived From SABER Observations

Ningchao Wang[1], Liying Qian[2], Jia Yue[3,4], Wenbin Wang[2], Martin G. Mlynczak[5], and James M. Russell III[1]

[1]Center for Atmospheric Sciences, Hampton University, Hampton, VA, USA, [2]High Altitude Observatory, National Center for Atmospheric Research, Boulder, CO, USA, [3]Catholic University of America, Washington, DC, USA, [4]NASA Goddard Space Flight Center, Greenbelt, MD, USA, [5]NASA Langley Research Center, Hampton, VA, USA

Key Points:

- Monthly climatology of the mesopause height, and MLT CO_2 gradients as signatures of the residual circulations are derived from SABER data
- Both the regions of maximum vertical CO_2 gradients and mesopause height show strong seasonal variations at mid-to-high latitudes
- Interannual variations of the height of maximum vertical CO_2 gradients and mesopause height are larger in the SH than in the NH

Correspondence to:

N. Wang,
NINGCHAO.WANG@hamptonu.edu

Citation:

Wang, N., Qian, L., Yue, J., Wang, W., Mlynczak, M. G., & Russell, J. M. III. (2022). Climatology of mesosphere and lower thermosphere residual circulations and mesopause height derived from SABER observations. *Journal of Geophysical Research: Atmospheres*, *127*, e2021JD035666. https://doi.org/10.1029/2021JD035666

Received 5 AUG 2021
Accepted 12 JAN 2022

Author Contributions:

Conceptualization: Ningchao Wang, Liying Qian, Jia Yue, Wenbin Wang
Formal analysis: Ningchao Wang
Investigation: Ningchao Wang
Methodology: Ningchao Wang, Liying Qian, Jia Yue, Wenbin Wang
Software: Ningchao Wang
Validation: Ningchao Wang
Writing – original draft: Ningchao Wang
Writing – review & editing: Liying Qian, Jia Yue, Wenbin Wang, Martin G. Mlynczak, James M. Russell III

Abstract In the mesosphere and lower thermosphere (MLT) region, residual circulations driven by gravity wave breaking and dissipation significantly impact constituent distribution and the height and temperature of the mesopause. The distribution of CO_2 can be used as a proxy for the residual circulations. Sounding of the Atmosphere using Broadband Emission Radiometry (SABER) CO_2 volume mixing ratio (VMR) and temperature measurements from 2003 to 2020 are used to study the monthly climatology of MLT residual circulations and the mesopause height. Our analyses show that (a) mesopause height strongly correlates with the CO_2 VMR vertical gradient during solstices; (b) mesopause height has a discontinuity at midlatitude in the summer hemisphere, with a lower mesopause height at mid-to-high latitudes as a result of adiabatic cooling driven by strong adiabatic upwelling; (c) the residual circulations have strong seasonal variations at mid-to-high latitudes, but they are more uniform at low latitudes; and (d) the interannual variability of the residual circulations and mesopause height is larger in the Southern Hemisphere (SH; 4–5 km) than in the Northern Hemisphere (NH; 0.5–1 km).

1. Introduction

Gravity waves originating from the troposphere propagate upward and break near the mesopause region (Holton & Joan Alexander, 1999). The breaking of gravity waves deposits momentum into the mesopause region and causes zonal wind reversal (Garcia & Solomon, 1985; Holton, 1983; Lindzen, 1981). Along with the Coriolis force, the gravity wave momentum deposition induces a mesospheric summer-to-winter residual circulation (Andrews & McIntyre, 1976). The mesospheric residual circulation causes a cold summer mesopause and a warmer winter mesopause through adiabatic cooling and warming, since the upwelling in the summer hemisphere causes adiabatic cooling, and the downwelling in the winter hemisphere causes adiabatic warming (Berger & von Zahn, 1999; States & Gardner, 2000; Xu et al., 2007). This mesospheric residual circulation has been well studied. For example, it is suggested that it is related to the double peaks of the mesopause that has two distinct altitudes and temperatures during the solstice: a lower (86–88 km) and colder mesopause in the summer hemisphere mid-to-high latitudes, and a higher (near 100 km) and warmer mesopause elsewhere. This phenomenon was observed and studied using Na lidars (She & von Zahn, 1998; von Zahn et al., 1996; Yu & She, 1995) and Sounding of the Atmosphere using Broadband Emission Radiometry (SABER) onboard the Thermosphere Ionosphere Mesosphere Energetics and Dynamics (TIMED) satellite (Xu et al., 2007).

Above the mesospheric residual circulation, there is a reverse winter-to-summer circulation in the lower thermosphere. High phase speed gravity waves can propagate into the lower thermosphere (see Figure 1 in Qian et al. [2017]); thus form a reverse winter-to-summer circulation in the lower thermosphere (e.g., Liu, 2007; Qian et al., 2017; Smith et al., 2011). Figure 1 shows the residual circulations in the mesosphere and lower thermosphere (MLT) region simulated by the Specified Dynamics Whole Atmosphere Community Climate Model (SD-WACCM) in (a) January and (b) July. There are three circulations in the MLT region during solstices: (a) a summer-to-winter mesospheric circulation below ∼95 km with upwelling in summer and downwelling in winter, (b) a lower thermospheric winter-to-summer circulation with upwelling in winter and downwelling in summer between ∼95 and ∼110 km, and (c) the bottom part of the thermospheric solar-driven summer-to-winter circulation with upwelling in summer and downwelling in winter above ∼110 km.

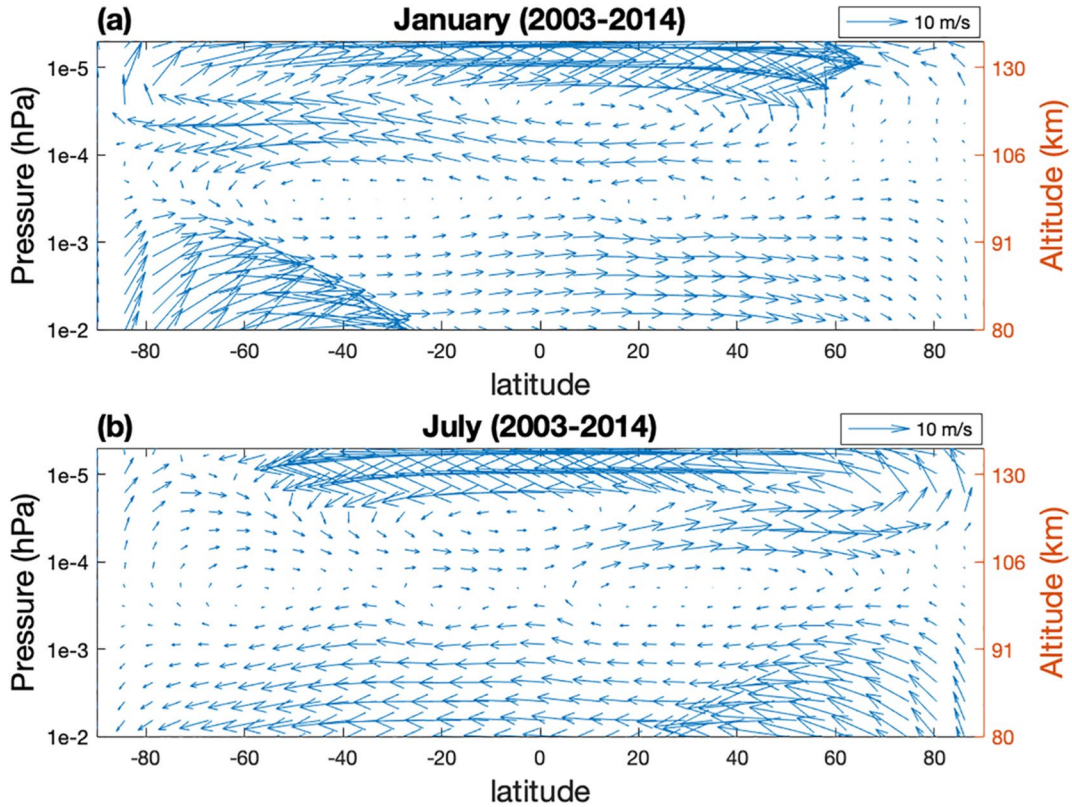

Figure 1. Specified Dynamics Whole Atmosphere Community Climate Model (SD-WACCM) simulations of the zonal mean wind fields (2003–2014) for (a) January and (b) July, which show the residual circulations in the mesosphere and lower thermosphere (MLT) region. The *y*-axis represents the pressure (left) in log scale in the unit of hPa, and the corresponding approximated altitude in km is marked on the right.

The lower thermospheric circulation significantly affects trace species distribution in the MLT region such as CO_2 (e.g., Rezac, Jian, et al., 2015; Smith et al., 2011). In addition, it has a significant impact on thermospheric atomic oxygen. Qian and Yue (2017) found that thermospheric O/N_2 decreased significantly in the winter hemisphere and increased slightly in the summer hemisphere due to the residual circulation-related upwelling in winter and downwelling in summer, respectively. By considering the lower thermospheric circulation effect in the Thermosphere Ionosphere Electrodynamics General Circulation Model (TIEGCM) simulations, the simulated O/N_2 latitudinal gradient and the ionospheric winter anomaly are more consistent with the Global Ultraviolet Imager (GUVI) observations. However, the residual circulations in the MLT are very difficult to observe directly, especially the lower thermospheric residual circulation. The lower thermosphere is dominated by diurnal and semidiurnal tides (Hagan & Forbes, 2002, 2003; Wu et al., 2008); the magnitudes of the residual circulation winds are substantially smaller than the tides (Qian & Yue, 2017).

CO_2 is a nonreactive species in the lower and middle atmosphere with a long chemical lifetime of hundreds of days. CO_2 originates in the troposphere and it is well mixed with a constant volume mixing ratio (VMR) from the source region to the mesosphere due to turbulent mixing and effect of the residual circulations. In the MLT region, the CO_2 distribution is predominantly controlled by horizontal and vertical transport (Kaufmann et al., 2002). Since the source of CO_2 is in the lower atmosphere and the chemical life time of CO_2 is long, CO_2 is an ideal dynamic tracer to visualize the residual circulations in the MLT region. In particular, atmospheric upwelling increases local CO_2 density, whereas downwelling decreases it. Thus, its spatial and temporal variations provide signatures of MLT residual circulations and their variabilities. In summer, the upwelling of the mesospheric circulation and the downwelling of the lower thermospheric circulation create a convergence zone of CO_2 with large CO_2 VMR vertical gradient. Consequently, CO_2 VMR vertical gradients maximize at the summer high latitudes (Qian et al., 2017).

Qian et al. (2017) derived the residual circulations in the MLT region using the CO_2 distribution observed by TIMED SABER and simulated by the SD-WACCM. They found that the maximum vertical gradient of CO_2 is at ∼95 km in the summer high latitudes, and it is at ∼106–110 km in the winter midlatitudes. The peak CO_2 gradient in summer high latitudes is due to the convergence of the upwelling of the mesospheric circulation and the downwelling of the lower thermospheric circulation. In the winter hemisphere, it is due to the convergence of the upwelling lower thermospheric circulation and the downwelling solar-driven thermospheric circulation. Therefore, the peak CO_2 gradient indicates the bottom boundary of the lower thermospheric circulation in summer and the top boundary of the lower thermospheric circulation in winter.

The aforementioned previous studies have demonstrated that mesospheric and lower thermospheric residual circulations play significant roles in the structure and variability of not only the mesopause temperature and height, and trace gas distributions in the MLT region, but also the thermospheric composition and ionospheric density (Qian & Yue, 2017; Qian et al., 2017). The residual circulations in the MLT region have been identified and studied via numerical simulations (Liu, 2007; Smith et al., 2011) and SABER measurements (Qian & Yue, 2017; Qian et al., 2017). However, to date, a climatological study of the residual circulations, especially the lower thermospheric residual circulation, is still not available. Understanding the interannual variation and seasonal variation of the residual circulations in the MLT region is of paramount interest.

In this paper, we, for the first time, derive the monthly climatology of the MLT residual circulations, using 18 years of continuous observations of CO_2 VMR by TIMED SABER, and study their seasonal and interannual variabilities. Since the residual circulations in the MLT region directly control the morphology of the vertical gradient of CO_2 VMR, the latter is used as a proxy for the residual circulations in this work. SABER temperature is also used to identify the mesopause temperature and height. The paper is organized as follows: we describe TIMED SABER temperature and CO_2 data in Section 2. We introduce the analysis method in Section 3. Then, we show the results in Section 4, followed by a discussion in Section 5 and brief summary in Section 6.

2. TIMED SABER Observations

The SABER instrument is onboard the NASA TIMED satellite which was launched on 7 December 2001 into a 74.1° inclination orbit at 630 km altitude with a period of 1.6 hr. TIMED SABER has retrieved temperature and O_3, O, CO_2, and H_2O profiles from ∼20 to ∼110 km since January 2002, with a vertical resolution of ∼2 km (Russell et al., 1999). The latitude coverage shifts between 83°N–53°S and 53°N–83°S, due to a ∼60-day yaw cycle of the TIMED satellite. SABER measures limb radiance in 10 broadband infrared channels including the CO_2 emission bands at 4.3 and 15 μm. A two-channel algorithm has been used to self-consistently and simultaneously retrieve the daytime kinetic temperature T_k and CO_2 VMR profiles, under nonlocal thermodynamic equilibrium (non-LTE) conditions in the altitude range of 65–110 km (Rezac, Jian, et al., 2015; Rezac, Kutepov, et al., 2015). The retrieved temperature error is ±2–3 K and the root sum square of the CO_2 VMR is between ±12 and ±21 ppmv for the altitude range studied in this work (Remsberg et al., 2008; Rezac, Kutepov, et al., 2015). More details of the SABER instrument and temperature and CO_2 VMR data retrieval can be found in Remsberg et al. (2008), Rezac, Kutepov, et al. (2015), and Russell et al. (1999).

3. Methods

In this work, we use SABER CO_2 VMR and temperature from 2003 to 2020. SABER CO_2 is used as a tracer to identify the convergence zones between the mesospheric residual circulation and the lower thermospheric residual circulation, and between the lower thermospheric residual circulation and the solar-driven thermospheric circulation. SABER temperature data are used to identify the mesopause temperature and location and to understand the height of the lower thermospheric circulation in relation to the mesopause height. The data in 2002 are not included in the analysis since SABER CO_2 VMR data start on day 32 of year 2002.

We first interpolate the temperature and CO_2 VMR measurements to a 1-km altitude grid ranging from 80 to 115 km. To obtain the monthly climatology of the residual circulations and the mesopause, we compute the zonal and monthly means of the CO_2 VMR and temperature in each 5° latitude bin from 80°S to 80°N, averaged over the years from 2003 to 2020. By taking the zonal and monthly average of the temperature and CO_2 VMR, nonmigrating tidal components are mostly removed or reduced (Xu et al., 2007). Note that since the SABER CO_2 VMR

is daytime only, the migrating tides in the CO_2 VMR cannot be removed. We identify the mesosphere height as the altitude of the coldest temperature in the altitude range from 80 to 100 km. We compare the mesopause height with the CO_2 VMR and its vertical gradient to study their correlation. The CO_2 VMR vertical gradient is defined as $\Delta CO_2/\Delta Z$, where the units of ΔCO_2 and ΔZ are ppmv and km, respectively. Note that in Qian et al. (2017), for the model–data comparison purpose (model is computed on pressure levels), they computed both simulated CO_2 VMR vertical gradient and the SABER CO_2 VMR vertical gradient as $\Delta CO_2/(-\Delta \log_{10} P)$, however, they computed the CO_2 VMR vertical gradient as $\Delta CO_2/\Delta Z$ to compare with the mesopause altitude. They found that the CO_2 VMR vertical gradient calculated in $\log_{10} P$ is larger than the CO_2 VMR vertical gradient calculated in altitude. In this work, since we analyze the relationship between the CO_2 VMR vertical gradient and the mesopause altitude, we defined the CO_2 VMR vertical gradient as $\Delta CO_2/\Delta Z$.

We then investigate the seasonal variability of the residual circulations and the mesopause at different latitudes. We selected four 20° latitudinal bands centered at 10°S and 10°N for low latitudes, and 50°S and 50°N for mid-to-high latitudes. The daily means for those latitude bands were computed for the CO_2 VMR and temperature for each year from 2003 to 2020. The average daily means were then calculated by averaging over all the years from 2003 to 2020.

Finally, we use a bimonthly (December–January and June–July) zonal mean in the high-latitude region (poleward of 50°N/S, 50°–80° in the summer hemisphere and 50°–60° in the winter hemisphere) during the solstices as a function of year from 2003 to 2020 to examine the interannual variations of the residual circulations and the mesopause height in both hemispheres. During the December solstice, we computed the zonal mean of CO_2 VMR vertical gradient and the temperature in December and January at 50°–80° latitude for the Southern Hemisphere (SH) and 50°–60° latitudes for the Northern Hemisphere (NH) for each year from 2003 to 2020. The vertical profiles of CO_2 VMR vertical gradient and the mesopause altitude were plotted as a function of year. During the June solstice, we processed the June and July CO_2 VMR and temperature data a similar way as we did for the December solstice, while the latitude range for the June solstice is 50°–80° for the NH and 50°–60° latitudes for the SH.

4. Results

Figure 2 shows the climatological distributions of CO_2 VMR (a and b), its vertical gradient (c and d), and temperature (e and f) in the MLT region, derived from SABER measurements, in January and July for the period from 2003 to 2020. The results in January are shown in the left column and the results in July are shown in the right column. The corresponding mesopause locations are shown as the white lines and black diamonds. Note that in Figures 2a–2d, there is no CO_2 data at high latitudes in the winter hemisphere. This is because SABER CO_2 VMR is retrieved for daytime only, and the solar zenith angle must be less than 80° to ensure a high signal-to-noise ratio (Rezac, Kutepov, et al., 2015). Consequently, there are no data at the winter high latitudes (>60°). However, this does not impair the study of the MLT circulations with the CO_2 measurements, as the SD-WACCM simulation results showed a good agreement with the SABER CO_2 between 0° and 54° in the winter hemisphere (cf., Figure 1 and Qian et al., 2017). Therefore, the SABER CO_2 VMR data should provide sufficient information on the MLT residual circulations in both the summer and winter hemispheres.

The altitude range of interest in this work is 80–115 km, which is above the CO_2 homopause between ∼70 and 80 km (Kaufmann et al., 2002; Qian et al., 2017). During January, temperature is colder at mid-to-high latitudes in the SH (Figure 2e). The mesopause altitude, which is defined as the coldest region in the mesosphere, varies from 90 km at 80°S with a minimum temperature of 139 K, to 86 km at 40°S with a minimum temperature of 180 K. The mesopause height shows a sudden jump to 97 km at ∼40°S, and then varies between 97 and 100 km from 35°S to 80°N. The minimum temperature in the mesosphere northward of 40°S is relatively constant compared to the minimum temperature at the mid-to-high latitudes in the SH.

The temperature variation in July (Figure 2f) is similar to the temperature variation in January (Figure 2e). The July temperature is colder at middle-to-high latitudes in the summer hemisphere (NH). The mesopause altitude varies from 90 km at 80°N with a minimum temperature of 129.1 K, to 83 km at ∼55°N with a minimum temperature of 160.9 K. The mesopause altitude is at 84 km between ∼55°N and 30°N. Between 25°N and 30°N, the mesopause height jumps from 84 to 97–99 km where it resides from 25°N to 80°S. In addition, at summer middle-to-high latitudes (NH for July and SH for January), the mesopause temperature is ∼10 K colder and the mesopause is

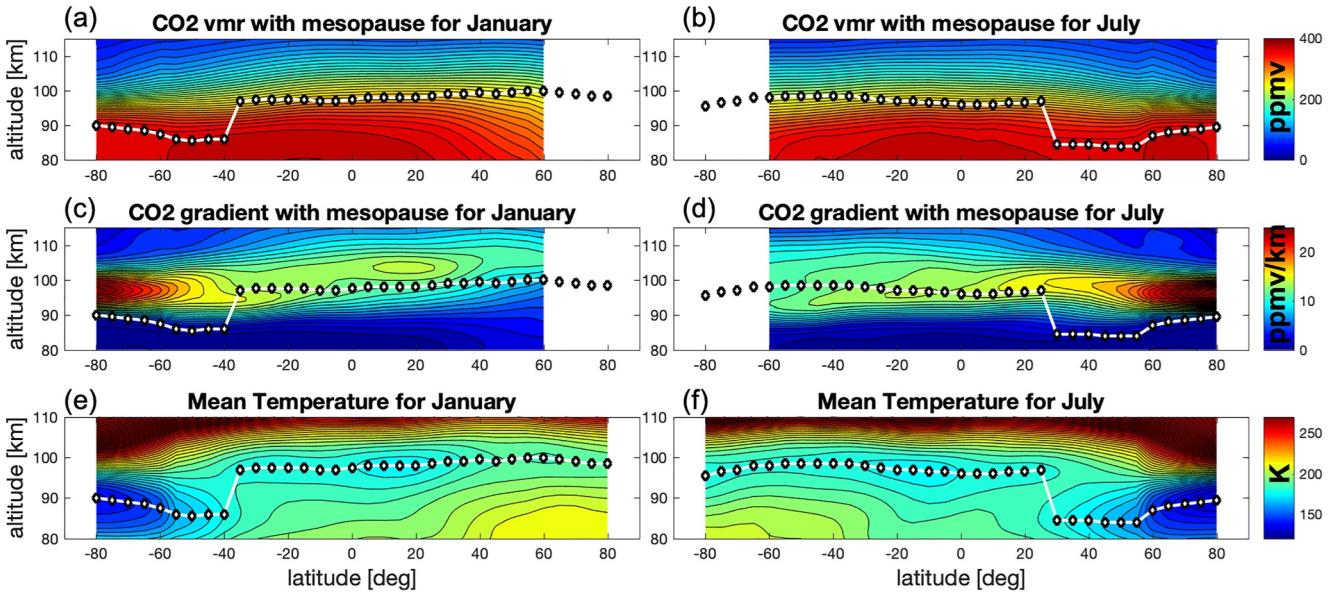

Figure 2. January (a, c, e) and July (b, d, f) monthly zonal averages of Sounding of the Atmosphere using Broadband Emission Radiometry (SABER) CO_2 volume mixing ratio in ppmv (a, b), CO_2 vertical gradient in ppmv/km (c, d), and temperature in degrees K (e, f) using data from 2003 to 2020. The white line with black diamonds in each panel represents the mesopause location at each corresponding 5° latitude bin.

~1–2 km lower in July than in January. This result is similar to Xu et al. (2007) who found that the mesopause during the June solstice is ~1 km lower and ~6–9 K colder than that during the December solstice. The possible reason for the difference between our result and the result of Xu et al. (2007) could be due to the different lengths of SABER temperature data set. In Xu et al. (2007), they used 4 years of SABER data from February 2002 to February 2006, while in this work, we used 18 years data from January 2003 to December 2020. The low summer mesopause height extend equatorward to a lower latitude (30°N) in July than in January (40°S). There is a hemispheric asymmetry between mesopause altitude and temperature during solstices, which is possibly caused by the asymmetry of the solar forcing and gravity wave forcing (Xu et al., 2007).

The CO_2 VMR isolines are closer together in the summer hemisphere (SH for January and NH for July) and more spread out in the winter hemisphere (NH for January and SH for July) (Figures 2a and 2b). The mesopause height follows the CO_2 VMR isolines at 90 km at mid-to-high latitudes in the summer hemisphere. At ~40°S in January and ~30°N in July, the CO_2 VMR isolines turn upward, the mesopause position has a jump of 12 km. The CO_2 VMR isolines are nearly horizontal in the tropical zone (20°S–20°N) and spread out at mid-to-high latitudes in the winter hemisphere.

The correlation between the CO_2 VMR and the mesopause height can be seen more clearly using the vertical gradient of CO_2 VMR. There is a regional maximum of CO_2 VMR vertical gradient at high latitudes in the summer hemisphere for both January and July, indicating convergence between the upwelling mesospheric residual circulation and the downwelling lower thermospheric residual circulation in this region. The sudden drops of the mesopause heights at ~40°S in January and ~30°N in July are closely related to the latitudinal boundaries of these intense convergence zones (Figures 2c and 2d), indicating that they are driven by dynamics. The altitude of the peak CO_2 vertical gradient moves from 97 km toward higher altitudes (105 km) from the summer (SH) to winter (NH) hemispheres in January, while in July, the altitude of the peak CO_2 gradients shows smaller variations from the summer (NH) to winter (SH) hemisphere. Since the CO_2 distribution is governed by the residual circulations in the MLT region, the July–January difference suggests that the hemispheric asymmetry not only exists in the mesopause altitude and temperature but also exists in the MLT residual circulations.

4.1. Monthly Climatology of the Residual Circulation Signature and Mesopause Height

The monthly climatology of CO_2 VMR vertical gradient and mesopause height from October to March (SH summer) and from April to September (NH summer) is shown in Figures 3 and 4, respectively. In each panel, the

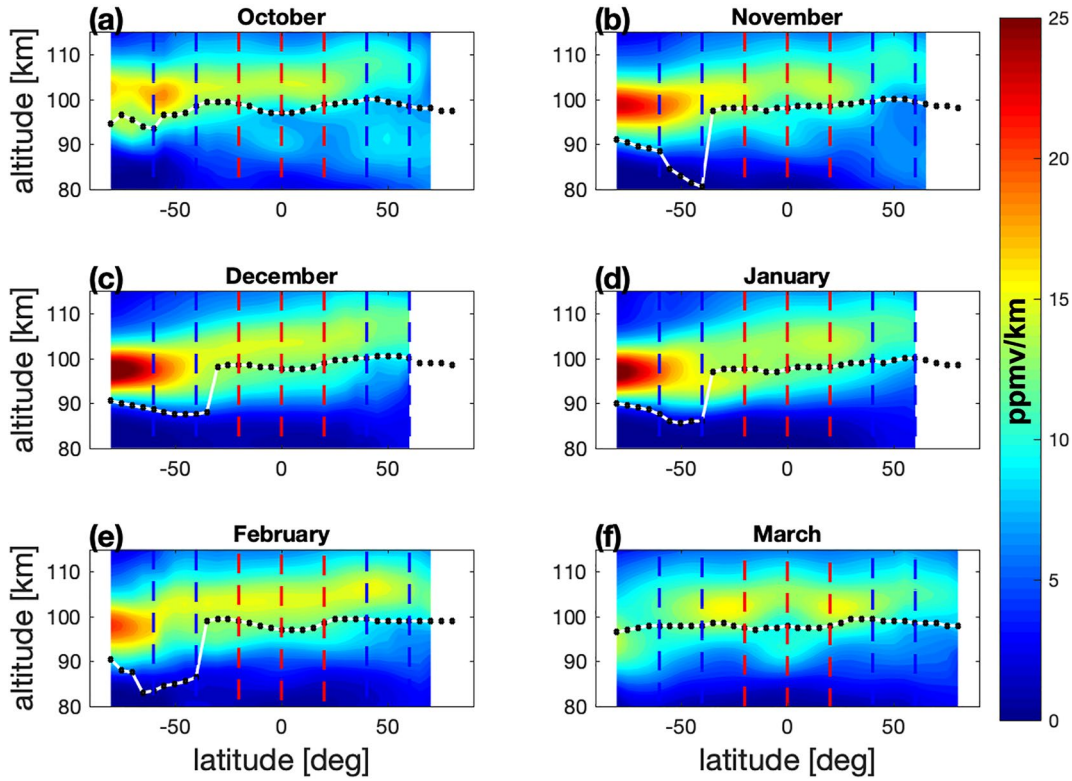

Figure 3. SABER monthly averaged CO_2 volume mixing ratio (VMR) vertical gradients with the corresponding mesopause locations for the months from October to March. The *x*-axis is latitude and *y*-axis is altitude. Colors represent the CO_2 VMR vertical gradient and the white line with black dots in each panel represents the mesopause location at each corresponding 5° latitude bin. The vertical blue and red dashed lines marked the 40°–60° and 0°–20° latitude regions in both hemispheres.

color contour represents the CO_2 VMR vertical gradient. The corresponding mesopause height is shown with the white line with black dots. Note that, for some months like April (Figure 4a), the CO_2 data do not extend to high latitude. This is due to the lack of CO_2 data. In April, there is less day time data due to the SABER measurement location.

The peak CO_2 VMR vertical gradients are larger during the solstices (>20 ppmv/km) than during the equinoxes (10–20 ppmv/km) in the polar region in the summer hemisphere (SH in Figure 3 and NH in Figure 4), which indicates that the vertical transport of CO_2 by the residual circulations is stronger during the solstices than during the equinoxes. The maximum magnitude of the CO_2 VMR vertical gradient increases from the equinoxes to the solstices (from Figure 3a/4a to Figures 3c and 3d, 4c and 4d) and then decreases from the solstices to the equinoxes (from Figures 3c and 3d, 4c and 4d to Figure 3f/4f) for both hemispheres, which suggests that the residual circulations become stronger from the equinox to the solstice, then becomes weaker from the solstice to the equinox, as expected.

The mesopause is at a constant altitude during the equinox months (Figures 3a and 3f/4a and 4f) and becomes discontinuous at the middle latitudes in the summer hemisphere (SH in Figure 3 and NH in Figure 4) from the equinoxes to the solstices (Figures 3b–3e and 4b–4e). As the vertical wind at the mid-to-high latitudes becomes stronger, the adiabatic cooling effects are stronger and cause a lower mesopause temperature and altitude. Figures 3 and 4 also show that the adiabatic cooling effects are strong enough to affect the mesopause altitude even during the transitional months (November, February, May, and August) between the equinoxes and the solstices.

4.2. Seasonal Variability of the Residual Circulation Signature and Mesopause Height

Figure 5 shows the daily average vertical gradients of SABER CO_2 VMR (color contours) and the corresponding mesopause locations (black dots) in the equatorial regions of (a) 10°N and (c) 10°S, and mid-to-high-latitude

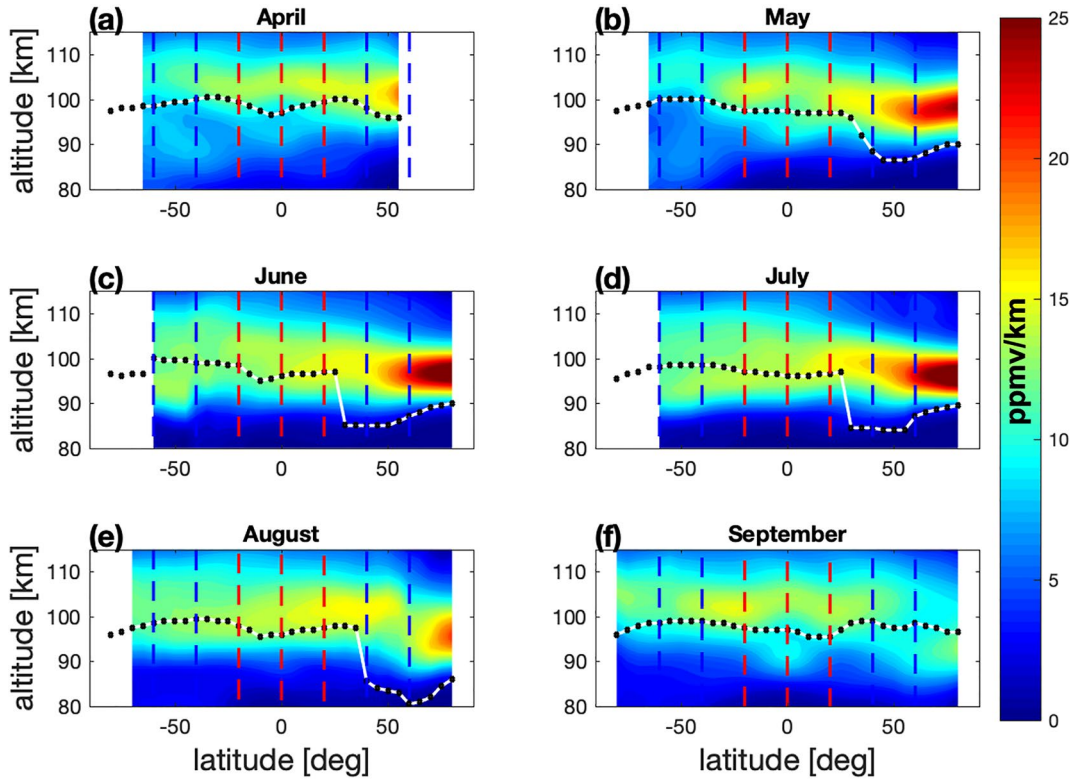

Figure 4. Same as Figure 3, but for the months from April to September.

regions of (b) 50°N and (d) 50°S within a 20° latitude band. The daily average is the mean of all the data from 2003 to 2020. Note that there are gaps at both low latitudes and mid-to-high latitudes. The gaps are due to the lack of the CO_2 VMR data. At low latitudes, the missing CO_2 VMR data are due to the change of yaw, while at mid-to-high latitudes, the missing CO_2 VMR data are due to local night, and large solar zenith angle (>80°).

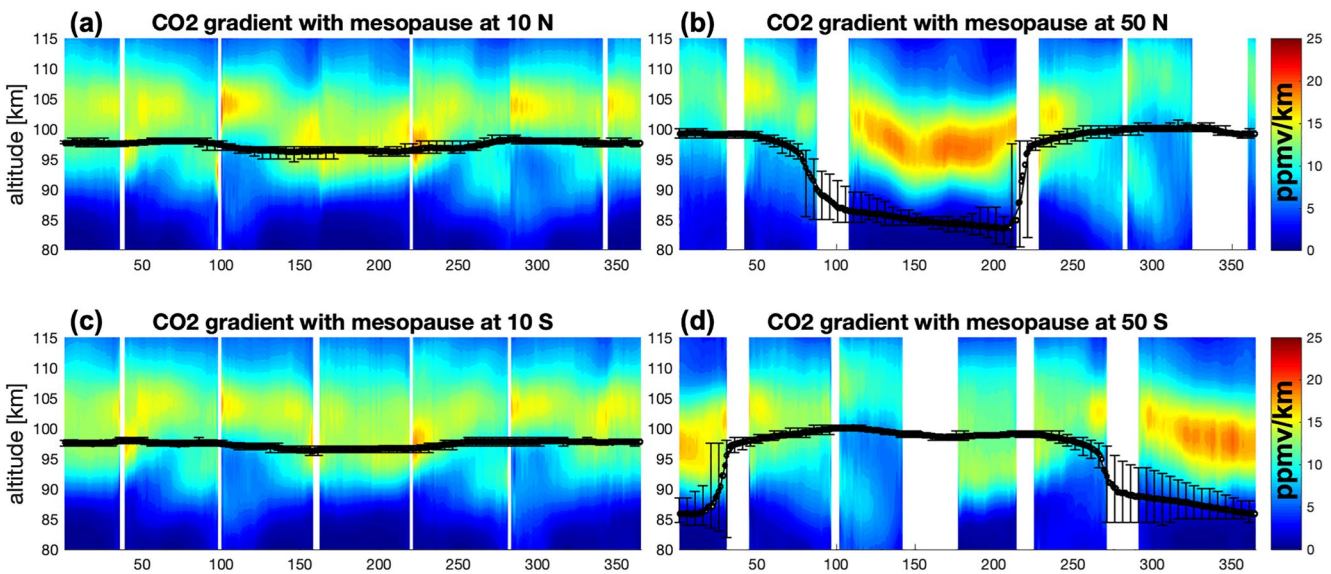

Figure 5. Daily average (2003–2020) vertical gradients of SABER CO_2 VMR (contours) and the mesopause location (black lines) for (a) 10°N, (b) 50°N, (c) 10°S, and (d) 50°S within 20° latitude bin. The *x*-axis is day of year (DOY) and the *y*-axis is the altitude from 80 to 115 km. The color contour represents the CO_2 VMR gradient ranging from −5 to 20. The vertical bars represent the interannual variations.

In the low-latitude region as shown in Figures 5a and 5c, the mesopause height varies between 96 and 98 km in both hemispheres. The maximum CO_2 VMR vertical gradient height varies from 97 to 103 km in both hemispheres. The height of maximum vertical gradients of CO_2 VMR is ~5 km above the mesopause. In lower latitude region (e.g., equatorial region), the residual circulations are nearly horizontal (as shown in Figure 1), so the mesopause altitude is at 97 km and is hardly affected by the adiabatic cooling/heating mechanism due to the vertical wind. The altitude of the peak CO_2 VMR vertical gradient at low latitudes may be caused by a combined effect of the turbulent and residual circulations. Since the residual circulations are horizontal at low latitudes and the vertical advection is nearly zero, there are no significant seasonal variations in the mesopause height and the location of the peak CO_2 VMR vertical gradient in this region. Further investigation is required to explore the mechanism that causes the altitude difference between the peak CO_2 VMR vertical gradient and the mesopause altitude, which is beyond the scope of this current work.

On the contrary, near 50°N/S, there are strong seasonal variations in both the mesopause height and the maximum CO_2 VMR vertical gradient altitude. In the NH mid-to-high latitudes (Figure 5b), the maximum CO_2 VMR gradient altitude begins to decrease at the end of February, on day of year (DOY) 50, dropping from 100 to 82 km, and then jumps back to 100 km at the end of July, on DOY 210. The maximum CO_2 VMR vertical gradient is larger during summer than in other seasons. The mesopause follows the trend of the altitude of the maximum CO_2 VMR vertical gradient. From January to the end of February (DOY 1 to DOY ~50), the mesopause is at a fixed altitude of ~100 km, and the mesopause altitude decreases significantly from March to mid-April (DOY ~60 to DOY ~100). The mesopause drops from 98 km at the beginning of March (DOY ~60) to 86 km in mid-April (DOY ~100). From mid-April to mid-July (DOY ~100–200), the mesopause drops from 86 to 82 km. At the end of July on DOY ~210, there is a discontinuity in the mesopause height. The mesopause jumps from 82 to 97 km in nearly 10 days, and after July (DOY ~210), the mesopause varies between 98 and 101 km. Similar phenomenon can be found in Xu et al. (2007). The altitude difference between the mesopause and the maximum CO_2 VMR vertical gradient is ~8 km from the September equinox to the March equinox. The altitude difference increases from the March equinox to the June solstice then decreases from the June solstice to the September equinox. The residual circulations become stronger, as well as the vertical wind at high latitudes, from the equinox to the solstice, thus the adiabatic cooling effect becomes stronger. The stronger adiabatic cooling effect causes a colder and lower mesopause, therefore the altitude difference becomes larger from the equinox to the solstice. On the contrary, from the solstice to the equinox, as the adiabatic cooling effect becomes weaker, the mesopause altitude moves to higher altitude, and the altitude difference between the peak of CO_2 VMR vertical gradient and mesopause height decreases. In April (on DOY ~110) the mesopause is ~13 km below altitude of the maximum CO_2 VMR gradient. During the June solstice, the mesopause is ~10 km below the maximum CO_2 VMR gradient. From the June solstice to the September equinox and to the December solstice, the height difference between the mesopause and the peak CO_2 VMR vertical gradient decreases to ~4–7 km. The seasonal variations of the CO_2 VMR vertical gradient and mesopause in the SH are similar to those in the NH. The mesopause and height of the peak CO_2 VMR vertical gradient are the lowest during the December solstice, and the altitude difference between the mesopause and the altitude of the peak CO_2 VMR vertical gradient is larger during the December solstice.

Figure 5 shows that the seasonal variations for both mesopause height and CO_2 VMR vertical gradient are stronger in mid-to-high latitudes than in the equatorial region in both hemispheres. To see more clearly how the magnitude and altitude of the CO_2 VMR vertical gradient vary throughout a year at low latitudes and mid-to-high latitudes, we compare the variations of the maximum CO_2 VMR vertical gradients and their altitudes in Figure 6. This analysis shows that the maximum CO_2 VMR vertical gradient and its altitude have stronger seasonal variations at high latitudes than at low latitudes. From the March equinox to the June solstice, at 50°N, the maximum CO_2 VMR vertical gradient increases from 12 to 20 ppmv/km, which is an increase of 67% in the NH. From the June solstice to the September equinox, the maximum gradient decreases from 20 to 12 ppmv/km. In the SH at 50°S, September equinox to December solstice, the maximum CO_2 VMR vertical gradient increases from 12 to 20 ppmv/km, then the maximum gradient decreases from 20 to 12 ppmv/km, from December solstice to March equinox. At 10° in both hemispheres, the variation of the CO_2 VMR maximum vertical gradient is between 13 and 17 ppmv/km throughout the whole year. There is an apparent variation of the CO_2 VMR maximum vertical gradient at low latitudes with a period of ~60 days. This is due to the TIMED 60-day yaw cycle during which SABER samples a full diurnal cycle.

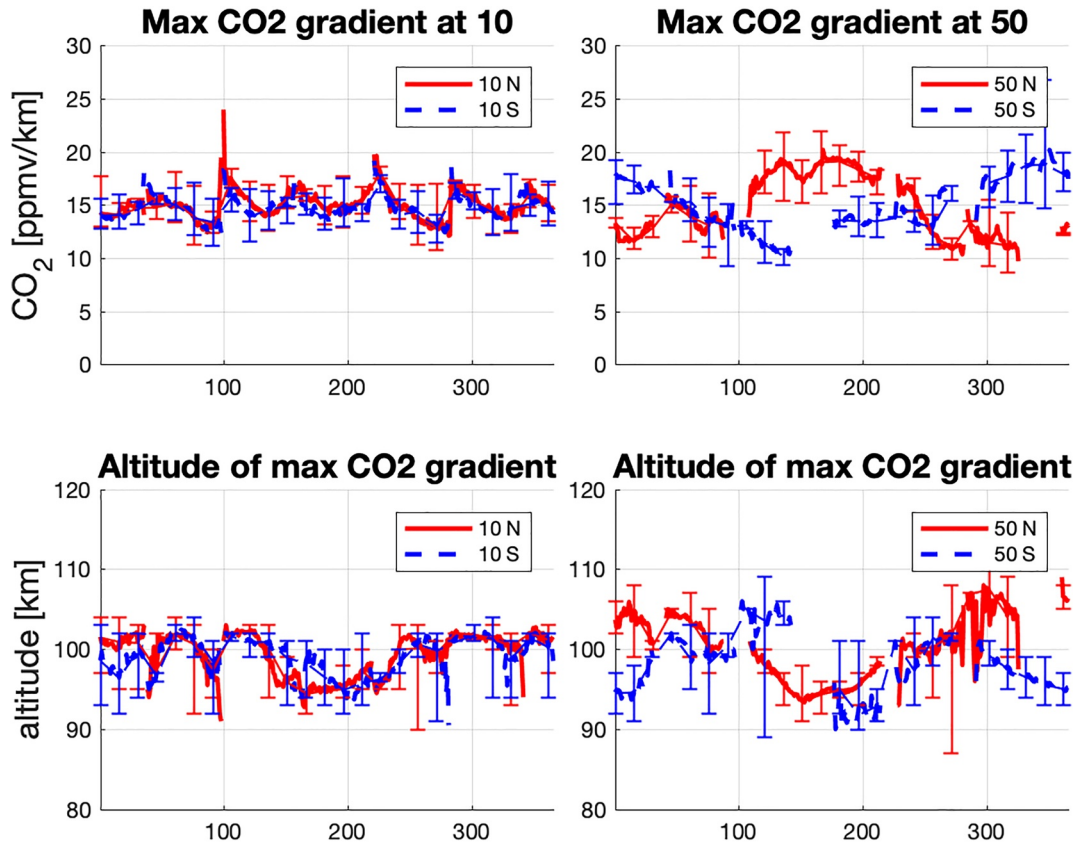

Figure 6. Seasonal variations of the CO_2 VMR maximum vertical gradient and its altitude within a 20°-latitude band centered at (a, c) 10°N/S; and at (b, d) 50°N/S. The red lines and dots show the results in the Northern Hemisphere and the blue lines and dots show the results in the Southern Hemisphere. The *x*-axis is day of year (DOY) for each panel. The *y*-axis is the vertical gradient value in the unit of ppmv/km for panels (a) and (b) and is altitude (km) for panels (c) and (d). The vertical bars represent the interannual variations.

At 50°N (Figure 6d), the altitude of the maximum CO_2 VMR vertical gradient varies from 100 km during the equinoxes to 95 km during the June solstice, and to 108 km during December solstice. At 50°S, the peak CO_2 VMR vertical gradient varies from 100 km during September equinox to 93 km during December solstice, and to 100 km during March equinox. However, during June solstice, the maximum CO_2 VMR vertical gradient appears at 90 km which is even lower than that during the December solstice. The altitude of the maximum CO_2 VMR vertical gradient is negatively correlated with the CO_2 VMR gradient maxima at high latitudes. The stronger the vertical gradient, the lower in altitude it is located. This negative correlation is stronger in the NH (−0.74) than in the SH (−0.58). The weak correlation in the SH is likely due to the lower CO_2 VMR vertical gradient peak height during the June solstice. In general, the peak CO_2 VMR vertical gradient is higher in the NH than in the SH. The altitude difference between the two hemispheres is larger during the winter solstice (December in the NH and June in the SH; ∼18 km) than during the summer solstice (June in the NH and December in the SH; ∼2 km). This hemispheric asymmetry is stronger in winter than in summer. At low latitudes, there is no strong correlation between the CO_2 VMR vertical gradient maxima and the altitude of the CO_2 VMR vertical gradient in both hemispheres.

4.3. Interannual Variability of the Residual Circulation Signature and Mesopause Height

Figure 7 shows the bimonthly zonal mean of the CO_2 VMR vertical gradient poleward of 50° latitudes for (a) austral winter (50°–60°S), (b) boreal summer (50°–80°N), (c) austral summer (50°–60°N), and (d) boreal winter (50°–80°S) from year 2003 to 2020. The corresponding mesopause location is shown as the black dotted white line. We compute the 2-month (December–January and June–July) average of the CO_2 VMR vertical gradient and mesopause altitude poleward of 50°N/S. For both hemisphere, the CO_2 VMR vertical gradient during summer is

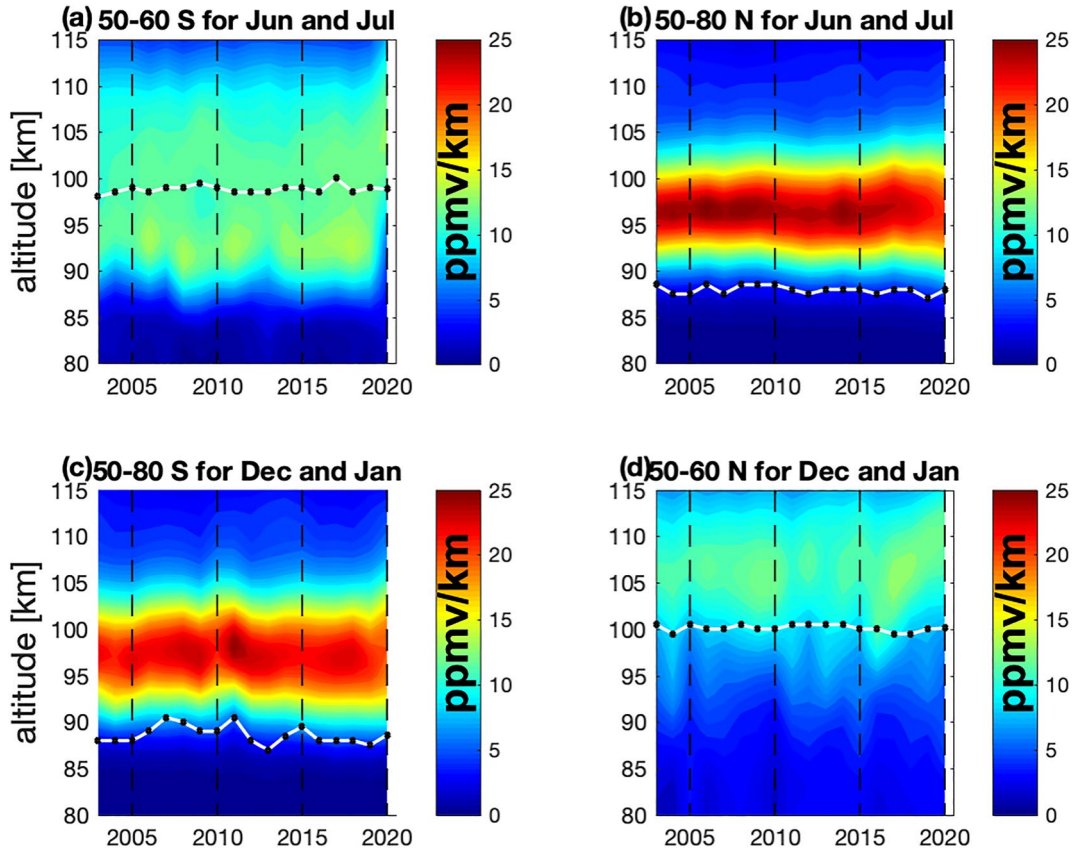

Figure 7. Bimonthly zonal average vertical gradients of SABER CO_2 VMR from 2003 to 2020 for (a) austral winter June and July at 50°–60°S, (b) boreal summer June and July at 50°–80°N, (c) austral summer December and January at 50°–80°S, and (d) boreal winter December and January at 50°–60°N. The *x*-axis is the year and the *y*-axis is the altitude. The color fill contour represents the vertical profile of CO_2 VMR vertical gradient for each year ranging from 0 to 25 ppmv/km, and the white line with black dots represents the mesopause location.

nearly 2 times larger than in winter; the mesopause is ∼10–15 km lower than the CO_2 VMR vertical gradient in summer; and the mesopause height in summer is also ∼10–15 km lower than the mesopause height during winter.

CO_2 vertical distribution is closely related to the vertical convections of the residual circulation. Thus, the magnitude and the altitude range of the CO_2 vertical gradient indicate the strength and the vertical range of the convergent zone created by the residual circulations. During June and July, the CO_2 VMR vertical gradient has a wider vertical distribution in the winter hemisphere (SH) than in the summer hemisphere (NH), which indicates that the convergent zone induced by the residual circulation has a wider altitude range in winter than in summer. For example, the CO_2 VMR vertical gradient that is larger than 10 ppmv/km (hereafter 10ppmv/km CO_2 VMR vertical gradient band) has a vertical range of 20 km from ∼90 to ∼110 km in the winter hemisphere (SH Figure 7a), whereas in the summer hemisphere (NH Figure 7b) the vertical range is 13 km from ∼90 to ∼103 km. As shown in Figure 7a (winter in the SH), the 10ppmv/km CO_2 VMR vertical gradient band has a width of ∼20 km in 2003, and the width of the band is ∼24 km in 2020. From 2003 to 2020, the width of the 10ppmv/km CO_2 VMR gradient band increases by 4 km. The altitude of the lower boundary of the 10ppmv/km CO_2 VMR vertical gradient band varies between 87 km in 2008 and 91 km in 2004 and 2013. The variation of the lower boundary altitude of the 10ppmv/km CO_2 VMR vertical gradient band has a negative correlation with the mesopause height, which varies from 95 km in 2004 to 99 km in 2008. The mesopause height has an increasing tendency from 2003 to 2020. As shown in Figure 7b (summer in the NH), the 10ppmv/km CO_2 VMR vertical gradient band has a width of ∼12 km in 2003, and the width of the band is ∼15 km in 2020. From 2003 to 2020, the width of the 10ppmv/km CO_2 VMR vertical gradient band increases by 3 km which is smaller than that in the SH winter. The altitude of the lower boundary of the 10ppmv/km CO_2 VMR vertical gradient band is consistently located at 90 km, and the mesopause height is at 88 km. Comparing the results in the two hemispheres, the CO_2 VMR vertical gradient and

the mesopause altitude have a smaller variation in the NH summer than in the SH winter. Note that in Figure 7a, the mesopause location is above the maximum CO_2 VMR vertical gradient. The large CO_2 VMR vertical gradient indicates the convergence zone created by the residual circulations. Below the convergence zone, the upwelling causes adiabatic cooling, however, the cooling effect is not strong enough to create a colder region below the mesopause. Thus, the mesopause is above the maximum CO_2 VMR vertical gradient. This phenomenon matches the results shown in Figure 5d.

During December and January, the CO_2 VMR gradient vertical distributions in the two hemispheres are similar. In the winter hemisphere (NH), the center altitude of the CO_2 VMR vertical gradient band is at ∼103–105 km which is ∼6–8 km higher than that in the summer hemisphere (∼97 km; SH). The mesopause height has a strong variation between 86 and 91 km in the summer hemisphere (SH). In the winter hemisphere (NH), the mesopause height is at ∼100 km.

Figure 7 shows that the interannual variability is stronger in the SH than in the NH for both the CO_2 VMR vertical gradient and the mesopause height. During the December and January (Figure 7c) in the SH, the mesopause has an altitude variation of 5 km, while during the June solstice in the NH, the mesopause is quasi-constant at 88 km with an altitude variation of 0.5 km, which indicates that the interannual variability of the residual circulation activity is stronger in the SH than in the NH. During the SH winter, the mesopause altitude range varies by ∼4 km, whereas the mesopause range in the NH winter varies by ∼1 km. Note that there is a distinguished difference in the winter hemisphere (NH for January and SH for July) between January and July. The CO_2 VMR and its gradient in July are similar to those in January in the summer hemisphere (SH for January and NH for July). However, in the winter hemisphere, the convergent zone driven by the lower thermospheric circulation and the solar-driven thermospheric circulation has a much wider altitude range and a lower mean altitude than the corresponding winter hemisphere convergence zone in January (e.g., Figures 7a and 7d). This winter convergence zone in July extends from 90 to 110 km with a peak at ∼92 km. This low altitude and wide CO_2 VMR convergent zone in the winter hemisphere in July can be seen in Figure 5d from DOY 180 to 220, and in Figure 7a.

5. Discussion

During solstices in the summer hemisphere, the maximum CO_2 VMR vertical gradient indicates the convergent zone driven by the mesospheric circulation and lower thermospheric circulation. Therefore, the altitude of the peak CO_2 VMR vertical gradient is the lower boundary of the lower thermospheric circulation in the summer hemisphere. There is another maximum CO_2 VMR vertical gradient region in the winter hemisphere at middle latitudes which represents the convergent region that is driven by the lower thermospheric residual circulation and thermospheric solar-driven circulation. Thus, the peak CO_2 VMR vertical gradient region indicates the upper boundary of the lower thermospheric circulation in the winter hemisphere. Note that the CO_2 VMR convergent zone has a much larger peak gradient in the summer hemisphere than in the winter hemisphere. This is due to the very strong upward transport by the mesospheric residual circulation in the summer high latitudes (Figure 1).

A hemispheric asymmetry can be found in both the mesopause height and the CO_2 VMR vertical gradient. Figure 2 shows that the mesopause temperature is ∼10 K colder and the mesopause is ∼1–2 km lower in SH during July than in NH during January, and the lower summer mesopause height extents equatorward to a lower latitude (30°N) in July than in January (40°S). The CO_2 VMR vertical gradient is larger in the SH high latitudes during July than in the NH high latitude during January. Moreover, the interannual variation poleward of 50° also has strong hemispheric asymmetry as the interannual variability is stronger in the SH than in the NH for both the CO_2 VMR vertical gradient and the mesopause height (Figure 7). The hemispheric asymmetries in the CO_2 VMR vertical gradient and the summer mesopause height are likely connected to the behavior of polar mesospheric clouds (PMCs) whose variability is greater in SH than in NH (Bailey et al., 2007). One of the possible reasons for this is interhemispheric coupling between the winter stratosphere and the summer mesosphere (Karlsson et al., 2007, 2009; Lieberman et al., 2021; Siskind et al., 2011), which is the process whereby planetary waves in the winter stratosphere drive anomalies in the residual circulation that give rise to anomalies in temperature that extend into the tropics and summer hemisphere. Thus, the asymmetry in planetary wave activity between the two hemispheres causes the difference in the mesospheric circulation (Becker & Schmitz, 2003; Karlsson et al., 2007). Since the residual circulations in the MLT region are driven by the breaking and dissipation of the gravity waves that is affected by planetary waves, the asymmetry in planetary wave activity can

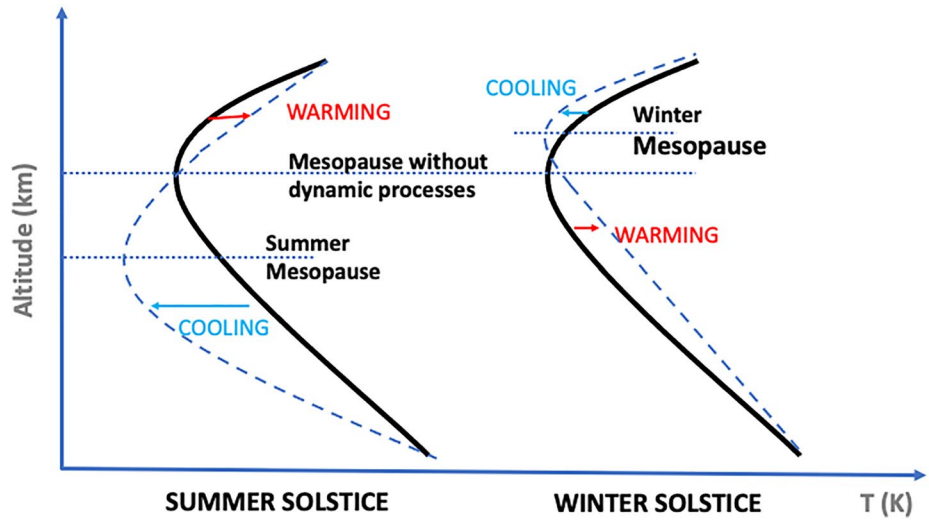

Figure 8. Schematic of the mesopause altitude variation at high latitudes during summer solstice (left) and winter solstice (right). The black curve lines represent the temperature profiles without considering the dynamic processes. The blue dashed curve lines represent the temperature profiles including the dynamical effects.

cause the asymmetry in residual circulations. The residual circulations affect the CO_2 distribution as well as the mesopause temperature and altitude, thus the hemispheric asymmetry in the residual circulations causes a hemispheric asymmetry in CO_2 VMR vertical gradient and the mesopause temperature and height. Further efforts are needed, such as diagnostic analyses, to explore the causes of the asymmetry in the residual circulations between January and July using first-principles whole atmosphere models, such as the Whole Atmosphere Community Climate Model with eXtend thermosphere and ionosphere (WACCM-X).

The upwelling in the summer hemisphere in the mesosphere induces adiabatic cooling and creates a cold summer mesopause at ~90 km at high latitudes, which is right below the mesospheric circulation at ~95 km as shown in Figures 2e and 2f. During the solstices, the mesopause appears at two different heights: ~90 km from mid-to-high latitudes in the summer hemisphere and ~100 km at other latitudes. There is a sharp drop in the mesopause altitude at middle latitudes in the summer hemisphere. The double-mesopause has been observed and studied with lidar measurements (She & von Zahn, 1998; von Zahn et al., 1996). The cold and lower mesopause at the mid-to-high latitudes in the summer hemisphere are caused by dynamical processes as shown in Figure 8. In the summer mesosphere, upwelling causes adiabatic cooling, whose effect is stronger at high latitudes. Thus, at high latitudes in the summer hemisphere, the adiabatic cooling effect induced by the upwelling of the mesospheric circulation creates a cooler and lower summer mesopause. At the mid-to-high-latitude region, the upwelling tendency is large as shown in Figures 2c and 2d, which induces large adiabatic cooling. Due to the cooling effect, the mesosphere temperature at ~90 km is colder than the temperature at ~100 km, therefore the mesopause moves to a lower altitude of ~90 km. Equatorward of this intense upwelling zone, the upwelling tendency in the mesosphere decreases and so does the adiabatic cooling effect. The cooling effect is not strong enough to create a colder temperature than the temperature at ~100 km, the mesopause remains at ~100 km. In general, the mesopause occurs at a lower altitude when the CO_2 VMR vertical gradient larger than 15 ppmv/km, and at a higher altitude when the CO_2 VMR vertical gradient below 15 ppmv/km, which indicates the residual circulations effects on the mesopause altitude. On the contrary, in the winter hemisphere, the upwelling of the lower thermospheric residual circulation causes cooling, and the downwelling of the mesospheric residual circulation causes warming, and thus a higher winter mesopause (Figure 8).

During the solstices in the summer hemisphere (June solstice for the NH Figure 7b and December solstice for the SH Figure 7c), there is a quasi-biennial oscillation (QBO) in the CO_2 VMR vertical gradient and the mesopause temperature for both hemispheres, however, the QBO during the solstices in the winter hemisphere (June solstice for the SH Figure 7a and December solstice for the NH Figure 7d) is not as obvious as that in the summer hemisphere. It is likely that during the solstices in the summer hemisphere, the CO_2 VMR is mostly governed by

the dynamical processes due to the stronger vertical winds compared to in the winter hemisphere (Figure 1). This needs to be tested with global model simulations and further observational evidence of gravity wave changes.

6. Summary

CO_2 VMR distribution provides direct signature of the MLT residual circulation patterns. We use CO_2 VMR and temperature measured by TIMED SABER from 2003 to 2020 to derive and analyze monthly climatology of the residual circulation signature in the MLT region and the mesopause height, and their seasonal and interannual variabilities. Our findings are as follows:

1. During solstices, the CO_2 VMR vertical gradients are larger in the high-latitude summer hemisphere driven by a strong convergence of the residual circulations in the region. The mesopause height follows the CO_2 VMR contour lines and stays below the peak of the CO_2 VMR vertical gradient at high latitudes in the summer hemisphere. The mesopause height has a discontinuity in the summer hemisphere, which occurs at ∼40°S in January, and ∼30°N in July: the mesopause height drops from 97 km at lower latitudes to 80 km at mid-to-high latitudes. This bimodal mesopause height distribution is in agreement with lidar observations (She & von Zahn, 1998; von Zahn et al., 1996). The mesopause height has a strong correlation with the CO_2 VMR vertical gradient. The mesopause occurs at a lower altitude when the CO_2 VMR vertical gradient larger than 15 ppmv/km, and at a higher altitude when the CO_2 VMR vertical gradient below 15 ppmv/km, reflecting residual circulation effects.
2. Monthly climatology reveal the residual circulation signatures as shown in the CO_2 VMR vertical gradient and the mesopause height for each month averaged from 2003 to 2020. During the months in the June solstice season, including May–August, CO_2 VMR vertical gradient at northern high latitudes is larger in magnitude and lower in altitude; at lower latitudes in the summer hemisphere and in the winter hemisphere, the magnitude becomes smaller and the altitude becomes higher. The opposite is true for the months in the December solstice season, including January, February, November, and December. The equinoxial months, including March, April, September, and October, show the transition features from one solstice season to the other. The mesopause height discontinuity at middle latitudes in the summer hemisphere occurs in all months except the four equinoxial months: March, April, September, and October.
3. CO_2 VMR vertical gradient and mesopause height show a strong seasonal variation at mid-to-high latitudes, but they are less variable at low latitudes indicating that vertical transport is stronger at higher latitudes than at lower latitudes.
4. The interannual variations of the residual circulation pattern and the mesopause height are stronger in the SH than in the NH. In addition, the CO_2 VMR vertical gradient belt becomes wider and the peak CO_2 VMR vertical gradient becomes smaller at high latitudes in the summer hemisphere from 2003 to 2020.
5. There is a distinguished difference in the convergent zone in the winter hemisphere between January and July. The convergent zone in July has a much wider altitude range and a lower mean altitude than the corresponding winter hemisphere convergence zone in January.

Data Availability Statement

SABER CO_2 VMR (V2.0, Level 2C) and temperature data (V2.0, Level 2A) since 2002 were downloaded from http://saber.gats-inc.com/data.php. SD-WACCM simulations shown in the paper are available at Zenodo at https://zenodo.org/record/5804538#.YehOiFjMK-o.

Acknowledgments
This work is supported by NSF AGS-1901126 and NASA AIM and TIMED/SABER missions, NASA HSR grants 80NSSC19K0835 and NNX17AI42G, and NASA NNX16AH06G, 80NSSC19K0278, and 80NSSC20K0189. The National Center for Atmospheric Research is sponsored by the National Science Foundation.

References

Andrews, D. G., & McIntyre, M. E. (1976). Planetary waves in horizontal and vertical shear: The generalized Eliassen–Palm relation and the mean zonal acceleration. *Journal of the Atmospheric Sciences*, *33*(11), 2031–2048. https://doi.org/10.1175/1520-0469(1976)033<2031:PWIHAV>2.0.CO;2

Bailey, S. M., Merkel, A. W., Thomas, G. E., & Rusch, D. W. (2007). Hemispheric differences in polar mesospheric cloud morphology observed by the student nitric oxide explorer. *Journal of Atmospheric and Solar-Terrestrial Physics*, *69*, 1407–1418. https://doi.org/10.1016/j.jastp.2007.02.008

Becker, E., & Schmitz, G. (2003). Climatological effects of orography and land–sea heating contrasts on the gravity wave–driven circulation of the mesosphere. *Journal of the Atmospheric Sciences*, *60*(1), 103–118. https://doi.org/10.1175/1520-0469(2003)060<0103:CEOOAL>2.0.CO;2

Berger, U., & von Zahn, U. (1999). The two-level structure of the mesopause: A model study. *Journal of Geophysical Research*, *104*(D18), 22083–22093. https://doi.org/10.1029/1999JD900389

Garcia, R. R., & Solomon, S. (1985). The effect of breaking gravity waves on the dynamics and chemical composition of the mesosphere and lower thermosphere. *Journal of Geophysical Research*, *90*(D2), 3850–3868. https://doi.org/10.1029/JD090iD02p03850

Hagan, M. E., & Forbes, J. M. (2002). Migrating and nonmigrating diurnal tides in the middle and upper atmosphere excited by tropospheric latent heat release. *Journal of Geophysical Research*, *107*(D24), 4754. https://doi.org/10.1029/2001JD001236

Hagan, M. E., & Forbes, J. M. (2003). Migrating and nonmigrating semidiurnal tides in the upper atmosphere excited by tropospheric latent heat release. *Journal of Geophysical Research*, *108*(A2), 1062. https://doi.org/10.1029/2002JA009466

Holton, J. R. (1983). The influence of gravity wave breaking on the general circulation of the middle atmosphere. *Journal of the Atmospheric Sciences*, *40*(10), 2497–2507. https://doi.org/10.1175/1520-0469(1983)040<2497:TIOGWB>2.0.CO;2

Holton, J. R., & Joan Alexander, M. (1999). Gravity waves in the mesosphere generated by tropospheric convention. *Tellus B: Chemical and Physical Meteorology*, *51*(1), 45–58. https://doi.org/10.3402/tellusb.v51i1.16259

Karlsson, B., Körnich, H., & Gumbel, J. (2007). Evidence for interhemispheric stratosphere–mesosphere coupling derived from noctilucent cloud properties. *Geophysical Research Letters*, *34*, L16806. https://doi.org/10.1029/2007GL030282

Karlsson, B., McLandress, C., & Shepherd, T. G. (2009). Inter-hemispheric mesospheric coupling in a comprehensive middle atmosphere model. *Journal of Atmospheric and Solar-Terrestrial Physics*, *71*, 518–530. https://doi.org/10.1016/j.jastp.2008.08.006

Kaufmann, M., Gusev, O. A., Grossmann, K. U., Roble, R. G., Hagan, M. E., Hartsough, C., & Kutepov, A. A. (2002). The vertical and horizontal distribution of CO_2 densities in the upper mesosphere and lower thermosphere as measured by CRISTA. *Journal of Geophysical Research*, *107*, 8182. https://doi.org/10.1029/2001JD000704

Lieberman, R. S., France, J., Ortland, D. A., & Eckermann, S. D. (2021). The role of inertial instability in cross-hemispheric coupling. *Journal of the Atmospheric Sciences*, *78*(4), 1113–1127. https://doi.org/10.1175/JAS-D-20-0119.1

Lindzen, R. S. (1981). Turbulence and stress owing to gravity wave and tidal breakdown. *Journal of Geophysical Research*, *86*(C10), 9707–9714. https://doi.org/10.1029/JC086iC10p09707

Liu, H. L. (2007). On the large wind shear and fast meridional transport above the mesopause. *Geophysical Research Letters*, *34*, L08815. https://doi.org/10.1029/2006GL028789

Qian, L., Burns, A., & Jia, Y. (2017). Evidence of the lower thermospheric winter-to-summer circulation from SABER CO_2 observations. *Geophysical Research Letters*, *44*, 10100–10107. https://doi.org/10.1002/2017GL075643

Qian, L., & Yue, J. (2017). Impact of the lower thermospheric winter-to-summer residual circulation on thermospheric composition. *Geophysical Research Letters*, *44*, 3971–3979. https://doi.org/10.1002/2017GL073361

Remsberg, E. E., Marshall, B. T., Garcia-Comas, M., Krueger, D., Lingenfelser, G. S., Martin-Torres, J., et al. (2008). Assessment of the quality of the version 1.07 temperature-versus-pressure profiles of the middle atmosphere from TIMED/SABER. *Journal of Geophysical Research*, *113*, D17101. https://doi.org/10.1029/2008JD010013

Rezac, L., Jian, Y., Yue, J., Russell, J. M., Kutepov, A., Garcia, R., et al. (2015). Validation of the global distribution of CO_2 volume mixing ratio in the mesosphere and lower thermosphere from SABER. *Journal of Geophysical Research: Atmospheres*, *120*, 12067–12081. https://doi.org/10.1002/2015JD023955

Rezac, L., Kutepov, A., Russell, J. M., Feofilov, A. G., Yue, J., & Goldberg, R. A. (2015). Simultaneous retrieval of T(p) and CO_2 VMR from two-channel non-LTE limb radiances and application to daytime SABER/TIMED measurements. *Journal of Atmospheric and Solar-Terrestrial Physics*, *130*(131), 23–42. https://doi.org/10.1016/j.jastp.2015.05.004

Russell, J., Mlynczak, M., Gordley, L., Tansock, J., & Esplin, R. (1999). An overview of the SABER experiment and preliminary calibration results. *Proceedings of SPIE*, *3756*, 277–288. https://doi.org/10.1117/12.366382

She, C. Y., & von Zahn, U. (1998). Concept of a two-level mesopause: Support through new lidar observations. *Journal of Geophysical Research*, *103*(D5), 5855–5863. https://doi.org/10.1029/97JD03450

Siskind, D. E., Stevens, M. H., Hervig, M., Sassi, F., Hoppel, K., Englert, C. R., & Kochenash, A. J. (2011). Consequences of recent southern hemisphere winter variability on polar mesospheric clouds. *Journal of Atmospheric and Solar-Terrestrial Physics*, *73*(13), 2013–2021. https://doi.org/10.1016/j.jastp.2011.06.014

Smith, A. K., Garcia, R. R., Marsh, D. R., & Richter, J. H. (2011). WACCM simulations of the mean circulation and trace species transport in the winter mesosphere. *Journal of Geophysical Research*, *116*, D20115. https://doi.org/10.1029/2011JD016083

States, R. J., & Gardner, C. S. (2000). Thermal structure of the mesopause region (80–105 km) at 40°N latitude. Part I: Seasonal variations. *Journal of the Atmospheric Sciences*, *57*(1), 66–77. https://doi.org/10.1175/1520-0469(2000)057<0066:TSOTMR>2.0.CO;2

von Zahn, U., Höffner, J., Eska, V., & Alpers, M. (1996). The mesopause altitude: Only two distinctive levels worldwide? *Geophysical Research Letters*, *23*(22), 3231–3234. https://doi.org/10.1029/96GL03041

Wu, Q., Ortland, D. A., Killeen, T. L., Roble, R. G., Hagan, M. E., Liu, H. L., et al. (2008). Global distribution and interannual variations of mesospheric and lower thermospheric neutral wind diurnal tide: 1. Migrating tide. *Journal of Geophysical Research*, *113*, A05308. https://doi.org/10.1029/2007JA012542

Xu, J., Liu, H. L., Yuan, W., Smith, A. K., Roble, R. G., Mertens, C. J., et al. (2007). Mesopause structure from Thermosphere, Ionosphere, Mesosphere, Energetics, and Dynamics (TIMED)/Sounding of the Atmosphere using Broadband Emission Radiometry (SABER) observations. *Journal of Geophysical Research*, *112*, D09102. https://doi.org/10.1029/2006JD007711

Yu, J. R., & She, C. Y. (1995). Climatology of a midlatitude mesopause region observed by a lidar at Fort Collins, Colorado (40.6°N, 105°W). *Journal of Geophysical Research*, *100*(D4), 7441–7452. https://doi.org/10.1029/94JD03109